Hydrodynamic theory of photon drag

John Eric Goff and W. L. Schaich
Department of Physics, Indiana University, Bloomington, Indiana 47405
(Received 24 June 1997)

We derive and evaluate a hydrodynamic theory of photon-drag effects in simple metals. Considering a jellium surface obliquely illuminated by monochromatic light, we calculate both the steady surface-parallel current and the emf induced along the surface normal. The sizes of these effects are estimated with a variety of approaches, ranging from momentum-balance arguments, through sum rules, to detailed microscopic calculations using a hydrodynamic description of the electrons' dynamics. Comparisons between the sometimes different results help clarify the physical origin of the phenomena, in particular, the extent to which effects are surface sensitive. We also outline a calculational approach that should allow a tractable incorporation of quantum-mechanical dynamics. [S0163-1829(97)04247-1]

I. INTRODUCTION

In this paper we consider a variety of ways to calculate photon-drag effects in simple metals. Our basic scheme is to adapt the hydrodynamic approach to second-harmonic generation[1] to treat the related problem of photon drag. If the light incident on the system is at frequency ω, its time variation can be represented by $\cos\omega t$, which also sets the variation of first-order response quantities. Second-order response quantities would then vary qualitatively as $\cos^2(\omega t)=\frac{1}{2}[1+\cos(2\omega t)]$. The $\cos(2\omega t)$ term describes the second-harmonic response, while the constant term describes the photon-drag response. From this point of view second harmonic and photon drag should be similar in regard to their physical origin and surface sensitivity. However, as we show here, detailed arguments and computations for the two classes of response can be quite different.

Many of these differences arise from how the second-order response reveals itself. In second-harmonic generation, and more generally sum-frequency generation,[2] the observable effect is radiation, whose intensity varies with the square of the second-order response. In contrast, with photon drag one is concerned with dc effects, either currents or emf's that have been induced in the conductor. These are directly proportional to the second-order response, and require either dc transport theory or static screening for their description, rather than radiation theory. Thus one ends up calculating quite different physical observables, which leads to different approximations, notation, language, etc. One of our goals in this work is to stress, where possible, common features between second-harmonic and photon-drag effects by using a model that can be applied to both.

Our model is jellium, which is reasonable for simple metals, and is where most first-principles calculations of second-harmonic generation have been done.[3–5] However, it strictly forbids interband transitions, which is the mechanism commonly used to describe photon drag. Most of this work has also been focused on semiconductors; see the book by Grinberg[6] for a review of the early efforts in bulk materials. Later, considerable effort was also made on semiconductor quantum-well systems, and only more recently on metallic conductors. See Ref. 7 for a brief review and a long list of references. Although most of this work has been built on (if theoretical) or interpreted with (if experimental) interband transitions, a model that only allows intraband transitions also produces photon-drag effects, and allows a tractable analysis of surface sensitivity, which is a particular interest for us. We describe the electrons' dynamics by using a phenomenological hydrodynamic equation of motion. As with the jellium model, this provides a crude but tractable description, and one that can be readily compared with second-harmonic calculations.[1]

We begin in Sec. II with formal arguments that avoid microscopic details. Similar arguments have been used by others before, in particular by Gurevich and coworkers,[8–10] and by Thellung.[11] The predictions of these arguments set the scale for comparisons with more involved treatments. We are able to show that in some special cases these arguments give the exact results for our model even though they fail in general. In Sec. III we develop the full microscopic solution. This involves not only expanding the equation of motion in a suitable series of orders, but also choosing the additional boundary conditions (ABC's) that are needed to obtain complete solutions. Then a sequence of model calculations is described which illustrates the range of behaviors that are possible. By varying conditions near the surface, we identify which parts of the calculation are surface sensitive. Finally, with an eye on future work, we show how our complete solution can be essentially reproduced by a simpler procedure which avoids retardation (and solving the full set of Maxwell's equations) in the numerical work.

II. MOMENTUM BALANCE ARGUMENTS

The following derivations are not rigorous, but instead suggestive of what to expect when a laser beam illuminates the flat surface of a thick conductor in which only intraband transitions are important (i.e., semi-infinite jellium). Let the angle of incidence of the wide light beam be θ. We ignore the effects due to the edges of the beam. The polarization of the light is not relevant for the general arguments, but is important for quantitative calculations. The incident Poynting flux along the beam direction is called S, and the mono-

chromatic light is assumed to have frequency ω.

First consider the light ''pressure'' (actually a shear stress) on the surface due to momentum transfer parallel to the surface. The flux of photons striking the surface is $(S/\hbar\omega)\cos\theta$. If a photon is reflected, it transfers no momentum parallel to the surface; while, if it is absorbed, a momentum $(\hbar\omega/c)\sin\theta$ is given to the metal. Hence the force per unit area parallel to the surface is

$$f_{\parallel}=\left(\frac{S}{\hbar\omega}\cos\theta\right)(1-R)\left(\hbar\frac{\omega}{c}\sin\theta\right)=\frac{S}{c}\sin\theta\cos\theta(1-R), \tag{1}$$

where R is the reflection coefficient.

We now argue that under steady-state conditions this rate of transfer of momentum from the light to the electrons near the surface must be balanced by resistive drag forces. Crudely representing these with a constant relaxation-time approximation, we write

$$f_{\parallel}=\int dx\frac{nmv_{\parallel}}{\tau}=\frac{m}{e\tau_b}\int dx(nev_{\parallel})=\frac{m}{e\tau_b}\int dx\ J_{\parallel}(x). \tag{2}$$

Here n is the density of electrons, and $v_{\parallel}$ is the component of their drift velocity parallel to the surface. The variable x runs along the surface normal, and the metal lies in $x>0$. Each electron has mass $m>0$ and charge $e<0$. The physical picture is that the electrons gain momentum by absorbing light, and lose momentum by resistive scattering, quickly settling into a steady drift parallel to the surface. Although a current is produced, no charge build-up occurs. The density of the parallel current, $J_{\parallel}$, varies with depth x, and vanishes beyond the penetration depth of the light fields and before the back side of the sample is reached. Our simple argument only produces the integral of $J_{\parallel}$ over x.

Combining Eqs. (1) and (2), we can express the result for the time-averaged current per unit length flowing parallel to the surface in several ways:

$$\int dx\langle J_{\parallel}\rangle=\left(\frac{e}{mc^2}\right)c\tau_b\langle S\rangle\sin\theta\cos\theta(1-R)$$

$$=\sigma_0\left(\frac{\langle S\rangle}{n_b ec}\right)\sin\theta\cos\theta(1-R). \tag{3}$$

Here angular brackets denote a time average, and with the free-electron mass $(|e|/mc^2)=1.96\ \mu$A/W. Also, σ_0 is the dc conductivity, $\sigma_0=n_b e^2\tau_b/m$, while $1/n_b ec$ is the free-electron Hall coefficient, both written in terms of the bulk electron density n_b. It is remarkable that although the current is a nonlinear response, one needs only linear-response properties to evaluate Eq. (3), which allows simple estimates of the magnitude of the photon-drag current.[8]

Before considering the limitations of the above derivation, let us briefly consider the response along the surface normal for which the argument changes in several ways. The projected incident flux is still $(S/\hbar\omega)\cos\theta$, but now even reflected photons transfer momentum to the metal. The light pressure normal to the surface is

$$f_{\perp}=\left(\frac{S}{\hbar\omega}\cos\theta\right)[(1-R)+2R]\left(\hbar\frac{\omega}{c}\cos\theta\right)=\frac{S}{c}\cos^2\theta(1+R), \tag{4}$$

where the two contributions in the square brackets are due to absorbed and reflected photons, respectively.[12] If we imagine an open circuit configuration, this light pressure causes a distortion of the electron charge density, which in turn induces an electric field whose force on the electrons counters the light pressure. We write

$$f_{\perp}=-\int dx\ neE_{\rm ind}=n_b e\Delta\mathcal{E}, \tag{5}$$

where $\Delta\mathcal{E}$ is the induced emf between below and above the surface. Combining Eqs. (4) and (5),

$$e\langle\Delta\mathcal{E}\rangle=\frac{\langle S\rangle}{n_b c}\cos^2\theta(1+R)$$

$$=\frac{\langle n_p\rangle}{n_b}\hbar\omega\cos^2\theta(1+R), \tag{6}$$

where n_p is the density of photons in the incident beam. One way to view this result is as a light-induced change in the work function. Alternatively if one can arrange for a current to flow in part along $\hat{x}$ through the region where $E_{\rm ind}\neq 0$ (see Ref. 13), then $\langle\Delta\mathcal{E}\rangle$ represents the light-induced emf in such a circuit.

Our results for the parallel and perpendicular response [Eqs. (3) and (6), respectively] are appealing for their simplicity, but suspect for the same reason. We assumed for the electrons that their equilibrium density and scattering rate are constant right up to the sharp edge of the surface. We have ignored the finite width of the light beam and the finite height of the electron surface barrier. Allowance for electron flow out of the illuminated region or out of the metal will complicate the analysis. The key idea of balancing rates of momentum transfer is not always valid, at least in the simple form we have applied it. Since free electrons cannot absorb photons, appropriate third bodies as sources of momentum should be considered. Yet in our argument the spatial inhomogeneity of the surface potential and/or of the scattering field responsible for $1/\tau$ were ignored.

To correct all these approximations is too difficult at present. However, with the aid of the hydrodynamic equation of motion, the consequences of several can be usefully examined. For the rest of this section we will outline an analysis which clarifies if and when the simple momentum-balance results, Eqs. (3) and (6), are reliable. Our method is based on combining moments of the hydrodynamic equation with Maxwell's equations to derive formal results (sum rules), which contain Eqs. (3) and (6) plus correction terms. In some cases we can prove that the correction terms are identically zero, while, in others, microscopic model calculations are needed to quantify the importance of the corrections.

The hydrodynamic model we use is defined by the following equation of motion for the electron velocity field $\vec{v}(\vec{x},t)$:

$$\frac{\partial \vec{v}}{\partial t}+(\vec{v}\cdot\vec{\nabla})\vec{v}=\frac{e}{m}\left[\vec{E}+\frac{1}{c}\vec{v}\times\vec{B}\right]-\frac{1}{mn}\vec{\nabla}p-\frac{1}{\tau}\vec{v}, \quad (7)$$

where $\vec{E}$ and $\vec{B}$ are electric and magnetic fields, respectively, and p is the pressure, which we assume depends only on the density n through $p=\zeta n^{5/3}$ with ζ a constant. Our approach to (approximately) solving Eq. (7) is based on expanding all variables there in a series of orders.

$$A=A_0+A_1+A_2+\cdots, \quad (8)$$

with $A\sim\vec{v},\vec{E},\vec{B},p,$ or n and generating a sequence of equations of fixed order.[1] Since the A_0 terms are equilibrium values, we assume that both $\vec{v}_0$ and $\vec{B}_0$ vanish. In this section we seek analogs of Eqs. (3) and (6), rather than a full microscopic solution. To this end introduce the charge density $\rho=ne$ and the current density $\vec{j}=ne\vec{v}$, and use the equation of continuity

$$\frac{\partial \rho}{\partial t}+\vec{\nabla}\cdot\vec{j}=0 \quad (9)$$

to rewrite the second-order version of Eq. (7) as

$$\left(\frac{\partial}{\partial t}+\frac{1}{\tau}\right)\ \vec{j}_2=-(\vec{j}_1\cdot\vec{\nabla})\vec{v}_1-(\vec{\nabla}\cdot\vec{j}_1)\vec{v}_1+\frac{e}{m}\left[\rho\vec{E}+\frac{1}{c}\ \vec{j}\times\vec{B}\right]_2-\frac{e}{m}\vec{\nabla}p_2. \quad (10)$$

The second-order contributions to the terms in the square brackets are

$$\left[\rho\vec{E}+\frac{1}{c}\vec{j}\times\vec{B}\right]_2=\rho_0\vec{E}_2+\rho_2\vec{E}_0+\left(\rho_1\vec{E}_1+\frac{1}{c}\vec{j}_1\times\vec{B}_1\right) \quad (11)$$

where the pieces within parentheses in Eq. (11) can be exactly rewritten[14] in terms of the light's momentum density

$$\vec{g}=\frac{1}{4\pi c}(\vec{E}_1\times\vec{B}_1), \quad (12)$$

and the Maxwell stress tensor

$$\overleftrightarrow{T}=\frac{1}{4\pi}[\vec{E}_1\vec{E}_1-\tfrac{1}{2}\ \overleftrightarrow{1}(\vec{E}_1\cdot\vec{E}_1)+\vec{B}_1\vec{B}_1-\tfrac{1}{2}\ \overleftrightarrow{1}(\vec{B}_1\cdot\vec{B}_1)] \quad (13)$$

as

$$\rho_1\vec{E}_1+\frac{1}{c}\vec{j}_1\times\vec{B}_1=-\frac{\partial\vec{g}}{\partial t}+\vec{\nabla}\cdot\overleftrightarrow{T}. \quad (14)$$

Substituting back into Eq. (10) and taking a time average, we obtain

$$\frac{m}{\tau e}\langle\vec{j}_2\rangle-\rho_0\langle\vec{E}_2\rangle=\langle\rho_2\rangle\vec{E}_0-2\vec{\nabla}\cdot\langle\overleftrightarrow{K}\rangle+\vec{\nabla}\cdot\langle\overleftrightarrow{T}\rangle-\vec{\nabla}\langle p_2\rangle, \quad (15)$$

where $\overleftrightarrow{K}=\frac{1}{2}mn_0\vec{v}_1\vec{v}_1$. The time average over the period $2\pi/\omega$ of the light has eliminated the second-harmonic parts of Eq. (10) and all time derivatives. The quantities in Eq. (15) are second-order, steady-state values. Although time independent, they are, in general, position dependent.

We are interested in the amount (at second-order) of current flowing parallel to the surface and the emf developed along the surface normal. These are defined by $\int dx\langle\hat{X}\cdot\vec{j}_2\rangle$ and $-\int dx\langle\hat{x}\cdot\vec{E}_2\rangle$, respectively, where $\hat{X}$ is a unit vector in the surface plane, and $\hat{x}$ is a unit vector along the surface normal. The integrands for these quantities can be discerned on the left-hand side of Eq. (15), while on the right-hand side are many derivative terms that can be integrated exactly. For the surface parallel current we find, if $\tau\to\tau_b$ independent of x,

$$\frac{m}{e\tau_b}\int dx\langle\hat{X}\cdot\vec{j}_2\rangle=2\langle\hat{X}\cdot\overleftrightarrow{K}(0)\cdot\hat{x}\rangle-\langle\hat{X}\cdot\overleftrightarrow{T}(0)\cdot\hat{x}\rangle. \quad (16)$$

We have also used a symmetry that, neglecting beam and sample (side) edge effects, implies that $\vec{E}_0,\langle\vec{E}_2\rangle$, and $\vec{\nabla}\langle p_2\rangle$ all point along $\hat{x}$. For the emf along the surface normal in an open circuit, we find, if $\rho_0\to\rho_b$ independent of x,

$$-\rho_b\int dx\langle\hat{x}\cdot\vec{E}_2\rangle=2\langle\hat{x}\cdot\overleftrightarrow{K}(0)\cdot\hat{x}\rangle-\langle\hat{x}\cdot\overleftrightarrow{T}(0)\cdot\hat{x}\rangle+\langle p_2(0)\rangle. \quad (17)$$

The reason the term with $\vec{E}_0$ does not contribute is because the zeroth-order form of Eq. (7) has $\vec{E}_0\propto\vec{\nabla}\rho_0$, which vanishes here since ρ_0 is presumed constant. For both Eqs. (16) and (17) we have assumed that all quantities become negligible deep in the bulk.

Equations (16) and (17) are close to Eqs. (3) and (6) if we note that $J_\parallel\sim\hat{X}\cdot\vec{j}_2$ and $E_{\rm ind}\sim\hat{x}\cdot\vec{E}_2$. It remains to evaluate at $x=0$ the terms on the right-hand side of Eqs. (16) and (17). We claim that the relevant elements of the kinetic-energy density tensor vanish because one requires $\hat{x}\cdot\vec{v}_1(0)=0$ to ensure that the first-order induced charge density at the surface be nonsingular. The contributions of the stress tensor elements are found from first-order field components. Since in the microscopic solution of the hydrodynamic model one also requires that all first-order fields be continuous through $x=0$, the evaluation of $\overleftrightarrow{T}$ is most easily done on the vacuum side of $x=0$, where only incident and reflected transverse waves are present. Call the projection of the incident light wave vector in the surface plane **Q**, and define a set of Cartesian axes by the triplet of unit vectors $(\hat{x},\hat{Q},\hat{t}=\hat{x}\times\hat{Q})$. Thus $\hat{x}$ and $\hat{Q}$ lie in the plane of incidence, and $\hat{t}$ is orthogonal to it. For either s- or p-polarized light, we find

$$\langle T_{tx}(0)\rangle=0, \quad (18)$$

$$\langle T_{Qx}(0)\rangle=-\frac{\langle S\rangle}{c}\cos\theta\,\sin\theta(1-R), \quad (19)$$

$$\langle T_{xx}(0)\rangle=-\frac{\langle S\rangle}{c}\cos^2\theta(1+R), \quad (20)$$

where R is the appropriate reflection coefficient. For a mixture of s- and p-polarized light, there are no cross-terms between the different polarizations, and one simply replaces R with $\alpha_pR^{(p)}+\alpha_sR^{(s)}$, where $\alpha_p+\alpha_s=1$, with $\alpha_p(\alpha_s)$ the

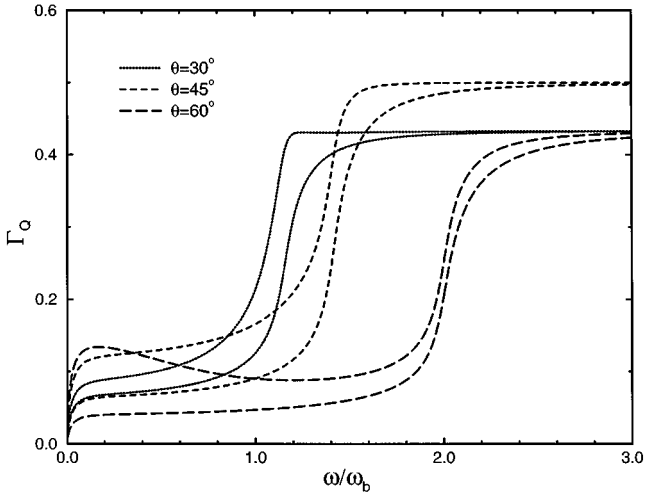

FIG. 1. Dimensionless photon-drag current parallel to the surface vs frequency for different angles of incidence in a one-step model. Results for p-polarized light lie everywhere above those for s-polarized light. Here $\Gamma_t \equiv 0$, and the momentum-balance prediction is exact.

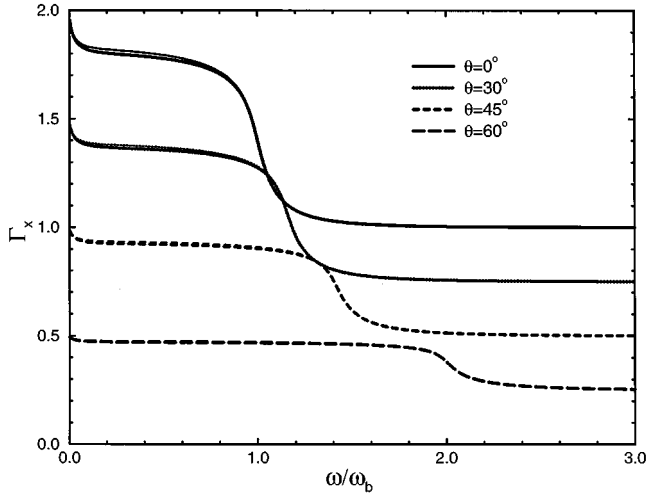

FIG. 2. Dimensionless photon-drag emf along the surface normal vs frequency for different angles of incidence in a one-step model. The incident light is s polarized. The thick curves are based on the full evaluation, Eq. (21), while the thin curves are from the simple momentum-balance result (6).

time-averaged fraction of the incident beam's flux polarized in (orthogonal to) the plane of incidence. For circularly polarized light $\alpha_p = \alpha_s = \frac{1}{2}$.

Thus for the current parallel to the surface we have, from Eqs. (16), (18), and (19), exactly reproduced Eq. (3). However, for the emf along the surface normal the implication of Eqs. (17) and (20) is that a correction term is missing from Eq. (6). One should write

$$e\langle \Delta \mathcal{E} \rangle = \frac{\langle S \rangle}{n_b c} \cos^2\theta (1+R) + \frac{\langle p_2(0) \rangle}{n_b}. \tag{21}$$

To quantify the size of this correction, we need to go beyond the formal manipulations used so far and carry through a full microscopic calculation to find $\langle p_2(x) \rangle$. This is a considerable effort and is described in Sec. III. Here we want to illustrate the numerical results before giving the algebraic detail.

The model system we evaluate has a bulk density described by $r_s = 2.07$, the value appropriate for Al. Results for different bulk densities, say $r_s \approx 4$ for Na, give qualitatively similar plots. The important energy scale is set by the bulk plasmon, which for Al has the value of $\hbar\omega_b = 15.8$ eV. The scattering time τ_b is set at $\omega_b \tau_b = 10$. In Fig. 1, we show the spectral dependence of the surface-parallel current in a one-step model, i.e., a model where ρ_0 and τ are each constant in the jellium. The dimensionless quantity plotted is defined by

$$\int dx \langle \hat{Q} \cdot \vec{j}_2 \rangle = \Gamma_Q \sigma_0 \left(\frac{\langle S \rangle}{n_b e c} \right), \tag{22}$$

and since the momentum-balance result is exact for a one-step model of the surface-parallel current, here $\Gamma_Q = \sin\theta \cos\theta \ (1-R)$. The structure in the plots is simply due to the drop in R from nearly 1 to nearly 0, as the frequency moves through the threshold for transparency of transverse waves in bulk at $\omega_b/\cos\theta$. The jump in Γ_Q sharpens as τ_b is increased. We remark that the total integrated current, $\int dx \langle \hat{Q} \cdot \vec{j}_2 \rangle$, tends as $\tau_b \to \infty$ to a nonzero, finite result over the frequency range where $1/\tau_b$ is necessary for optical absorption. This range extends up to $\omega_b/\cos\theta$ for incident s waves, but only up to ω_b for p waves. The upper-frequency limit is set by the threshold for plasmon creation.

The similarity between s and p waves evident in Fig. 1 is lost when we examine the emf induced along the surface normal. Results are shown for the one-step model in Figs. 2 and 3 for incident s and p waves, respectively. In both figures the dimensionless quantity plotted is defined by

$$-e \int dx \langle \hat{x} \cdot \vec{E}_2 \rangle = \Gamma_x \left(\frac{\langle S \rangle}{n_b c} \right). \tag{23}$$

If the momentum balance result were exact, Γ_x would be $\cos^2\theta(1+R)$. This is nearly true for the s wave case, but is

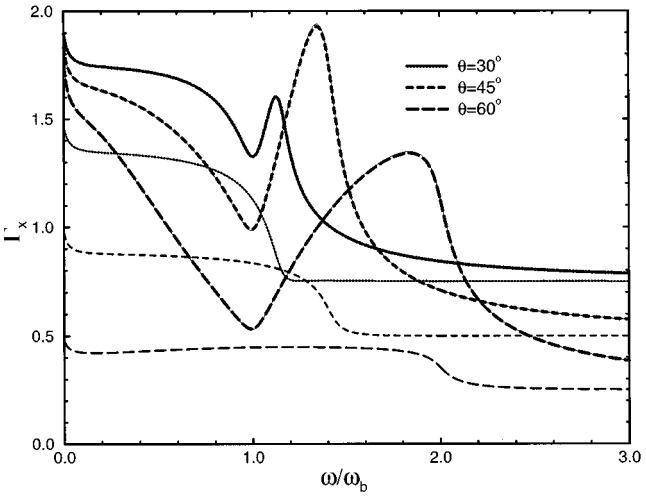

FIG. 3. Same as Fig. (2), except here the incident light is p polarized. The results for $\theta = 0$ are omitted since they are the same as those in Fig. 2. The thin solid lines are based on Eq. (58).

clearly wrong for p waves. For the latter case the last term in Eq. (21) is a significant correction, and completely changes the spectral dependence. In Sec. III we delve further into the microscopic details in order to understand the physics behind this interesting structure. We will also find that the relatively simple appearance of the Γ's in Figs. 1 and 2 can be considerably modified if one goes beyond a one-step model of the metal surface.

III. MICROSCOPIC CALCULATIONS

In this section we derive and evaluate microscopic expressions for the photon-drag response. Within the hydrodynamic model such calculations are fairly straightforward, so we concentrate on questions of principle and numerical results.

A. Basic equations

The formal analysis is quite similar to that developed for second-harmonic generation by Corvi and Schaich (CS).[1,15] One begins by expanding Eq. (7) into a series of orders—see Eqs. [CS—4(a)–4(c)]. From the zeroth-order equation, a relation between $\vec{E}_0$ and the gradient of ρ_0 is obtained (CS-7):

$$\vec{E}_0=\frac{4\pi\beta_0^2}{\omega_0^2}\vec{\nabla}\rho_0, \tag{24}$$

where $\omega_0^2=4\pi n_0 e^2/m$ and $\beta_0^2=\frac{5}{3}\zeta n_0^{2/3}/m$. We will choose the parameter ζ so that

$$\beta_0^2=\tfrac{3}{5}\,v_F^2 \tag{25}$$

with v_F the Fermi velocity of a uniform free-electron gas of density n_0. This allows an accurate description of the bulk plasmon dispersion.[16] Next we use Eq. (24) to eliminate $\vec{E}_0$ from the higher-order equations of motion. At first order this leads to Eq. (CS-8),

$$\left(\frac{\partial}{\partial t}+\frac{1}{\tau}\right)\vec{v}_1=\frac{e}{m}\vec{E}_1-\vec{\nabla}\left(\frac{\beta_0^2}{\rho_0}\rho_1\right). \tag{26}$$

For our model calculations we shall assume that n_0 and $1/\tau$ have a steplike dependence on the surface-normal coordinate x. In order to decide what ABC's to impose across planes where n_0 and/or $1/\tau$ have discontinuities, our criteria are to require that all electromagnetic field components be continuous and to suppress singularities in other physical quantities as much as possible. Since we have the freedom to choose only two ABC's at an internal interface (where n_0 is nonzero on both sides of the interface) and just one ABC at the external interface (with vacuum), our options are rather limited. To supplement Eq. (26), we impose continuity of $[(\beta_0^2/\rho_0)\rho_1]$ at each internal interface, which keeps $\hat{x}\cdot\vec{v}_1$ from being singular. Similarly, to keep ρ_1 nonsingular (and $\hat{x}\cdot\vec{E}_1$ continuous), we require the continuity of $\hat{x}\cdot\vec{j}_1$ from Eq. (9) at all interfaces. These first-order ABC choices are the same as used by CS. Note that, although they ensure the continuity of several quantities (all components of $\vec{E}_1$ and $\vec{B}_1$, $\hat{x}\cdot\vec{j}_1$) for another set of quantities (ρ_1, surface-parallel components of $\vec{j}_1$, all components of $\vec{v}_1$, and normal derivatives of any component of $\vec{E}_1$ and $\vec{B}_1$), they in general only suppress singularities, not discontinuities. These limitations cause trouble at second-order.

The useful analog of Eq. (26) in second-order is Eq. (CS-10),

$$\left(\frac{\partial}{\partial t}+\frac{1}{\tau}\right)\vec{v}_2=\frac{e}{m}\left[\vec{E}_2+\frac{1}{c}\vec{v}_1\times\vec{B}_1\right]-(\vec{v}_1\cdot\vec{\nabla})\vec{v}_1 -\vec{\nabla}\left[\frac{\beta_0^2}{n_0}\left(n_2-\frac{1}{6}\frac{n_1^2}{n_0}\right)\right]. \tag{27}$$

Again, with an eye on Eq. (9), we impose at all interfaces continuity of $\hat{x}\cdot\vec{j}_2$ to keep ρ_2 nonsingular and $\hat{x}\cdot\vec{E}_2$ continuous. The remaining ABC at internal interfaces is used to suppress the singularities associated with the normal derivative of discontinuous quantities. Specifically, we require continuity of

$$\tfrac{1}{2}(\hat{x}\cdot\vec{v}_1)^2+\frac{\beta_0^2}{\rho_0}\left(\rho_2-\frac{1}{6}\frac{\rho_1^2}{\rho_0}\right). \tag{28}$$

Note that, if τ is continuous, Eq. (26) implies that the surface-parallel components of $\vec{v}$ are continuous too. Our second-order ABC's then are equivalent to those of CS. But if τ is discontinuous at an internal interface (which CS did not allow), the ABC's proposed here are different. In particular, at a discontinuity in τ, there is a singularity in the surface-parallel components of $(\vec{v}_1\cdot\vec{\nabla})\vec{v}_1$, which implies a δ-function contribution to the induced second-order current density.

This complication is an unappealing feature of our model solution. It would not arise if we did not allow discontinuities in τ and n_0.[17,18] But if τ and n_0 vary smoothly with x, one loses the convenient option of matching plane-wave solutions across various interfaces, and must numerically integrate the equations of motion over all x. In our opinion this extra effort is not justified in an initial analysis. It would seem more appropriate to make such a computational investment later for a more sophisticated model, one that goes beyond hydrodynamics to better treat the electrons' dynamics with quantum mechanics.

The hydrodynamic equations we need to solve in regions of constant n_0 and τ are, at first order [Eq. (CS-9)],

$$\left(\frac{\partial}{\partial t}+\frac{1}{\tau}\right)\vec{j}_1=\frac{\omega_0^2}{4\pi}\vec{E}_1-\beta_0^2\vec{\nabla}\rho_1, \tag{29}$$

and, at second-order [Eq. (CS-13)],

$$\left(\frac{\partial}{\partial t}+\frac{1}{\tau}\right)\vec{j}_2=\frac{\omega_0^2}{4\pi}\vec{E}_2-\beta_0^2\vec{\nabla}\rho_2+\vec{R}, \tag{30}$$

where the nonlinear driving terms

$$\vec{R}=\frac{e}{mc}(\vec{j}_1\times\vec{B}_1)-(\vec{j}_1\cdot\vec{\nabla})\vec{v}_1+\left(\frac{\partial}{\partial t}+\frac{1}{\tau}\right)\left(\frac{\rho_1}{\rho_0}\vec{j}_1\right) +\frac{\rho_1}{3\rho_0}\beta_0^2\vec{\nabla}\rho_1 \tag{31}$$

are bilinear in first-order quantities. These equations are to be solved together with Maxwell's equations and the equation of continuity. Up to this point, our theory applies equally well to photon drag and second-harmonic generation. We now break this generality by taking a time average of Eq. (30) to extract the steady-state terms

$$\frac{1}{\tau}\langle\vec{j}_2\rangle=\frac{\omega_0^2}{4\pi}\langle\vec{E}_2\rangle-\beta_0^2\vec{\nabla}\langle\rho_2\rangle+\langle\vec{R}\rangle, \tag{32}$$

with

$$\langle\vec{R}\rangle=\frac{e}{mc}\langle\vec{j}_1\times\vec{B}_1\rangle-\langle(\vec{j}_1\cdot\vec{\nabla})\vec{v}_1\rangle+\left\langle\frac{\rho_1}{\rho_0}\left(\frac{1}{\tau}\vec{j}_1+\frac{\beta_0^2}{3}\vec{\nabla}\rho_1\right)\right\rangle. \tag{33}$$

Note that the last average in Eq. (33) involves different functions from Eq. (CS-14).[19]

The quantities of interest in photon drag are readily found from Eqs. (32) and (33). First note that, by symmetry, the vectors $\langle\vec{E}_2\rangle$ and $\vec{\nabla}\langle\rho_2\rangle$ can only point along the surface normal. Hence the density of surface parallel current is simply

$$\langle\hat{X}\cdot\vec{j}_2\rangle=\tau\langle\hat{X}\cdot\vec{R}\rangle. \tag{34}$$

There is no screening of these components. Along $\hat{x}$, matters are slightly more complicated. By symmetry, $\langle\hat{x}\cdot\vec{j}_2\rangle$ can only depend on x, and by the equation of continuity must in fact be constant. For an open circuit configuration, where $\langle\hat{x}\cdot\vec{j}_2\rangle$ vanishes in vacuum, our ABC of continuous $\langle\hat{x}\cdot\vec{j}_2\rangle$ implies then that $\langle\hat{x}\cdot\vec{j}_2\rangle$ is identically zero. We are left with the (static) screening problem

$$\left(\frac{\partial^2}{\partial x^2}-\kappa_0^2\right)\langle\hat{x}\cdot\vec{E}_2\rangle=\frac{4\pi}{\beta_0^2}\langle\hat{x}\cdot\vec{R}\rangle, \tag{35}$$

where we used Gauss's law to eliminate $\langle\rho_2\rangle$. The screening wave vector that appears here, $\kappa_0^2=\omega_0^2/\beta_0^2$, is set by the choice (25). To change it to the more physically appealing Thomas-Fermi value would require replacing $\beta_0^2\rightarrow\frac{1}{3}v_F^2$. Since photon drag mixes behaviors at high and low frequencies, there is no obvious way with a single choice of β_0^2 to describe both extremes appropriately.[20]

We use the method of partial waves to produce explicit solutions.[1] In each region of constant n_0 and τ, the general solution is written as a linear combination of plane waves. Their coefficients are determined by matching with the standard and additional boundary conditions across each plane of discontinuity in n_0 and/or τ. At first order the plane waves have the common frequency ω and surface-parallel wave vector $\mathbf{Q}$. They are distinguished by whether they are longitudinal or transverse, and by whether they propagate parallel or antiparallel to $\hat{x}$. For a real-valued, space- and time-dependent vector $\vec{A}_1(\vec{x},t)$, we write

$$\vec{A}_1(\vec{x},t)=\mathrm{Re}[\vec{A}_1(x)e^{i(\mathbf{Q}\cdot\mathbf{X}-\omega t)}], \tag{36}$$

where Re [ ] denotes ''real part of'' and the complex amplitude $\vec{A}_1(x)$ describes the polarization and propagation direction (along $\hat{x}$) of the wave. Note that the convention in Eq. (36) differs by a factor of 2 from Eq. (CS-15). For the time averages needed in Eq. (33), we have the rule

$$\langle A_1(\vec{x},t)B_1(\vec{x},t)\rangle=\tfrac{1}{2}\mathrm{Re}[A_1^*(\vec{x})B_1(\vec{x})]. \tag{37}$$

With these definitions we can outline how one completes the calculation of $\int dx\langle\hat{X}\cdot\vec{j}_2\rangle$ and $-\int dx\langle\hat{x}\cdot\vec{E}_2\rangle$. For the surface-parallel current we simply use Eq. (34) for the integrand. The only point worth further discussion is how to handle the singularity in $\tau\langle\hat{X}\cdot\vec{R}\rangle$ if τ is discontinuous. The singular contribution arises from $-\frac{1}{2}\,\mathrm{Re}\,[\tau(\hat{x}\cdot\vec{j}_1(x))^*(\partial/\partial x)\langle\hat{X}\cdot\vec{v}_1(x)\rangle]$, where, from Eq. (26),

$$\hat{X}\cdot\vec{v}_1(x)=\left[\frac{e}{m}\hat{X}\cdot\vec{E}_1(x)-i\hat{X}\cdot\mathbf{Q}\left(\frac{\beta_0^2}{\rho_0}\rho_1(x)\right)\right]\Big/\,(-i\omega+1/\tau). \tag{38}$$

The numerator in Eq. (38) is continuous, as is $(\hat{x}\cdot\vec{j}_1(x))^*$. Hence if the jump in τ occurs at x_0 we have, for the integral over the singularity,

$$\int_{x_0^-}^{x_0^+}dx\;\;\tau\langle\hat{X}\cdot\vec{R}\rangle=-\frac{\mathrm{Re}}{2}\left\{(\hat{x}\cdot\vec{j}_1(x_0))^*\left[\frac{e}{m}\hat{X}\cdot\vec{E}_1(x_0)-i\hat{X}\cdot\mathbf{Q}\left(\frac{\beta_0^2}{\rho_0}\rho_1(x_0)\right)\right]I\right\}, \tag{39}$$

where

$$I=\int_{x_o^-}^{x_o^+}dx\;\;\tau\frac{\partial}{\partial x}\left(-i\omega+\frac{1}{\tau}\right)^{-1}. \tag{40}$$

Assuming τ varies monotonically from $\tau^-=\tau(x_0^-)$ to $\tau^+=\tau(x_0^+)$, we find, as $x_0^\pm$ tends to x_0 from above and below, that

$$I=\Delta\left\{\frac{1}{\tilde{\omega}^2}-\frac{1}{\omega^2}\ln(1-i\omega\tau)\right\}, \tag{41}$$

where $\tilde{\omega}^2=\omega(\omega+i/\tau)$ and Δ denotes ''discontinuity in.''

For the emf along the surface normal, the integrand $\langle\hat{x}\cdot\vec{E}_2\rangle$ is nonsingular, but we must first solve the screening problem (35). In any step region of constants n_0 and τ, we can write, from Eq. (33),

$$\langle\hat{x}\cdot\vec{R}\rangle=\tfrac{1}{2}\mathrm{Re}\left[\sum_j\;R_je^{-Q_jx}\right], \tag{42}$$

where both complex amplitudes R_j and the complex wave vectors Q_j are known in terms of first-order quantities. We then write in this same step region,

$$\langle\hat{x}\cdot\vec{E}_2\rangle=\tfrac{1}{2}\mathrm{Re}\left[\frac{4\pi}{\beta_0^2}\sum_j\;\frac{R_j}{Q_j^2-\kappa_0^2}\;\;e^{-Q_jx}\right]+\lambda_+e^{\kappa_0x}+\lambda_-e^{-\kappa_0x}. \tag{43}$$

Each step region has a pair of $\lambda_\pm$ terms, except the bulk, where the λ_+ coefficient is set to zero. These coefficients of homogeneous solutions of Eq. (35) are determined by imposing the second-order boundary conditions. Specifically,

we require continuity of both $\langle \hat{x}\cdot\vec{E}_2\rangle$ and the time average of Eq. (28) at each internal interface. We assume that the second-order electric field vanishes in vacuum; i.e., that the total induced charge at second order $\int dx\langle\rho_2(x)\rangle=0$. Our final ABC is hence that $\langle \hat{x}\cdot\vec{E}_2(0^+)\rangle=0$. This set of constraints allows all the λ's to be found, and then one can trivially integrate Eq. (43). For a one-step model only one λ term is needed and we can write the screened second-order field in $x>0$ as

$$\langle \hat{x}\cdot\vec{E}_2\rangle=\tfrac{1}{2}\mathrm{Re}\left[\frac{4\pi}{\beta_0^2}\sum_j \frac{R_j}{Q_j^2-\kappa_0^2}(e^{-Q_j x}-e^{-\kappa_0 x})\right]. \quad (44)$$

To check the sum rule result (21), we need

$$\langle p_2(0)\rangle=\frac{m\beta_0^2}{e}\left(\langle\rho_2(0)\rangle+\frac{1}{3}\,\frac{\langle\rho_1^2(0)\rangle}{\rho_0}\right). \quad (45)$$

Here $\rho_1(x)$ is determined solely by the first-order calculation, and vanishes if the incident beam is pure s wave. For $\langle\rho_2(0)\rangle$, we apply Gauss's law to Eq. (43).

B. Model calculations

We now return to numerical examples. We will concentrate on double-step models, wherein either the equilibrium density or the scattering rate is modified from its bulk value over a thin layer of width w of order Å at the surface. We will also mostly show results for incident light that is p polarized, since these spectra show the richest structure and greatest surface sensitivity. Results for s-polarized light remain quite similar to those plotted in Figs. 1 and 2. The physical reason for this distinct behavior is because at first-order s-polarized light does not induce any longitudinal waves in the metal. The spatial variations along $\hat{x}$ are then set by transverse wave vectors such as

$$p_T=\frac{\omega}{c}\,(\epsilon-\sin^2\theta)^{1/2}, \quad (46)$$

where c is the speed of light and ϵ is the (local) dielectric constant, $\epsilon=1-\omega_0^2/\tilde{\omega}^2$ with ω_0 either a bulk or surface value. For our choices of selvedge width w, $|p_T w|\ll 1$. The only nonzero driving term in Eq. (33) for s waves is from the Lorentz force. It is slowly varying, and extends far into the bulk because its associated Q_j there [see Eq. (42)] is given by $2\,\mathrm{Im}(p_T)\ll\kappa_0$ with Im( ) meaning ''imaginary part of.'' There is consequently little screening of this driving field except near (on the scale of w) the surface, which has hardly any effect on its integral over x. We have made plots of the surface-parallel current and emf along the surface normal [described by Γ_Q of Eq. (22) and Γ_x of Eq. (23), respectively] for s waves incident on a general double-step model. Although the results do not agree with the momentum-balance predictions in Eqs. (3) and (6), the deviations are small and smooth functions of frequency.[21] Hence there is little evident surface sensitivity, and one can essentially reproduce plots of s-wave Γ's using local optics and a single-step model.

Matters are more interesting with incident p waves, where induced surface charges in both first and second-order result in longitudinal fields that are large and short ranged (i.e., surface sensitive). In Fig. 4 we show results for Γ_x for the standard[16,22] double-step model of Al. The selvedge width is 4 Å, and the equilibrium density there is 0.7 that in bulk. We use $\omega_b\tau=10$ at all x. Compared to Fig. 3, there is additional structure both below and above ω_b. The common peak for all angles of incidence at $\omega/\omega_b\sim 0.88$ is due to a multipole plasmon, which in a hydrodynamic model can be simply viewed as a plasmon trapped in the selvedge.[23] The location of this peak is a sensitive function of w and n_s, the selvedge value of n_0. We found that its frequency position in Γ_x correlates well with the nonretarded $\mathbf{Q}=\mathbf{0}$ multipole eigenfrequency.[24] It also correlates well with the location of an extra peak in the reflection coefficient $R^{(p)}$. The latter peak is a much smaller structure (changing $R^{(p)}$ by just a few percent), but is the only extra structure in the surface-parallel current compared to Fig. 1.[21] For Γ_x this peak, as well as those due to scattering resonances above ω_b, produce much larger effects than they do for $R^{(p)}$. This emphasizes that the momentum-balance prediction (6) is not even qualitatively valid for Γ_x with p-polarized light.

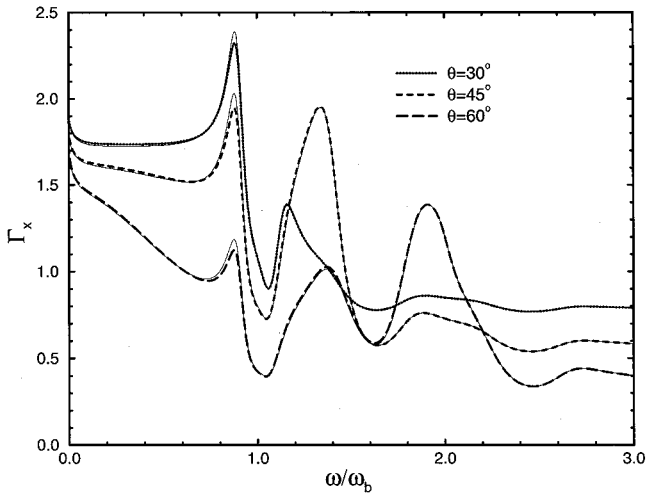

FIG. 4. Dimensionless photon-drag emf along the surface normal vs frequency for different angles of incidence in a double-step model. The incident light is p polarized and only the equilibrium density is stepped. The thin solid lines are based on Eq. (58).

Next consider the response when one holds the equilibrium density constant, but allows the scattering rate to be changed near the surface. For the emf along the surface normal we find curves for Γ_x, which are similar to those in Fig. 3. Increasing the scattering rate near the surface broadens the structures, while reducing $1/\tau$ sharpens them. The curves remain significantly different from the momentum-balance prediction (6), but these differences are fundamentally due to the correction term in Eq. (21), not the changes in τ. However, when we examine the surface-parallel current in a model with constant n_0 and variations in τ, the deviations from Eq. (3) are controlled by the scattering rates. Some results for Γ_Q are shown in Fig. 5. For simplicity we keep the selvedge width at 4 Å and use $\omega_b\tau_b=10$, but the value of τ in the selvedge, τ_s, is varied. Note that over a range of frequencies below ω_b, the sign of Γ_Q can be changed if the surface scattering rate is increased. This is a clear indication

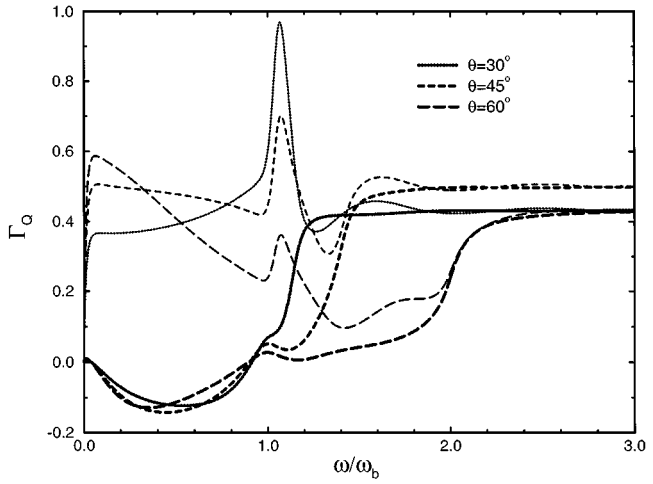

FIG. 5. Dimensionless photon-drag current parallel to the surface vs frequency for different angles of incidence in a double-step model. The incident light is p polarized and only the scattering rate is stepped: $1/\tau_s$ is 5 (0.2) times $1/\tau_b$ for the thick (thin) curves.

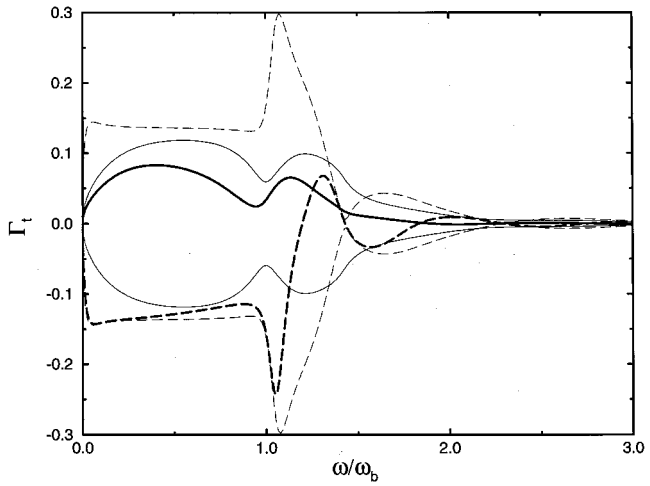

FIG. 6. Dimensionless photon-drag current orthogonal to the plane of incidence vs frequency in a double-step model. The light is incident at 45° and is linearly polarized at 45° to the plane of incidence. Only the scattering rate is stepped and the solid (dashed) curves are for $1/\tau$ being 5 (0.2) times $1/\tau_b$. The two pair of thin curves bound the range of possible values for different phase relations between the s and p components of the incident light.

that the momentum-balance prediction (3) no longer applies. To understand this behavior one needs to consider the microscopic variation of the driving terms in Eq. (33). For p-polarized light all the terms are nonzero,[25] but not necessarily of the same sign even if τ is constant. The net current is determined by

$$\int dx\langle \hat{Q}\cdot\vec{j}_2\rangle = \int dx\ \tau(x)\langle \hat{Q}\cdot\vec{R}(x)\rangle, \tag{47}$$

so we can imagine changing the sign of the integral by using variations in (positive) τ to differently weight the sign-varying $\langle \hat{Q}\cdot\vec{R}(x)\rangle$. In more physical terms, the strength *and* direction of the driving force exerted on the electrons by the light varies with depth into the metal. In our simple model one may view via Eq. (47) electrons at depth x as responding locally to the driving force at that depth. So if we allow the electrons a longer scattering time at those depths where the driving force is in one direction, and a shorter one over the depths where the driving force is in the opposite direction, we can ''engineer'' the direction in which the net current flows.

One can further exploit this idea to produce a nonzero surface-parallel current orthogonal to the plane of incidence. In Fig. 6 we plot Γ_t defined by

$$\int dx\langle \hat{t}\cdot\vec{j}_2\rangle = \Gamma_t\sigma_0\left(\frac{\langle S\rangle}{n_b e c}\right) \tag{48}$$

for the same model as used in Fig. 5. If one has pure p or s polarization in the incident light, then $\langle \hat{t}\cdot\vec{R}\rangle$ is identically zero. But if we mix the two polarizations, $\langle \hat{t}\cdot\vec{R}\rangle$ becomes nonzero, although for constant τ its integral over x remains zero. Hence, if we use τ to give uneven weights, we can remove cancellations in the integral (48) and find a nonzero Γ_t. The value of Γ_t depends not only on the magnitudes of the s and p components of the polarization, but also on their relative phase. For the results shown by the thick curves in Fig. 6 the projection of the net polarization direction is positive on both the $\hat{x}$ and $\hat{t}$ axes, which we describe by a phase angle of $\varphi=0$. If φ is varied between 0 and π, the net polarization changes from linear, to circular, and back to linear (but orthogonal to the starting direction). The range of Γ_t values that could be obtained by such variations ($0\leqslant\varphi\leqslant 2\pi$) are bounded by the thin curves in Fig. 6. Note that the magnitude of Γ_t, which depends on the failure of the momentum-balance prediction (3), is noticeably smaller than Γ_Q's of Fig. 1. We also remark that it is only for Γ_t (and with τ not constant[21]) that one finds a ''mixing'' contribution between s and p polarizations. Neither Γ_Q nor Γ_x depends on the phase angle φ.

C. Alternate calculational scheme

In preparation for work on more sophisticated models, we seek a way to simplify the computational effort. Our goal is to establish an analog of the shortcuts used in second-harmonic generation.[26] The basic idea is to evaluate long-range contributions analytically using full retardation, and to calculate short-range contributions numerically using nonretarded expressions, where by contributions we mean the various parts of the driving field $\langle \hat{x}\cdot\vec{R}\rangle$ of Eq. (33). We consider only $\langle \hat{x}\cdot\vec{R}\rangle$ (and Γ_x) because we are looking toward models where $1/\tau$ is constant, and hence the momentum balance result (3) will hold for surface-parallel currents.

The long-range contributions are those terms in Eq. (33) whose spatial variation in bulk is set by the transverse wave vector p_T of Eq. (46). Their amplitudes are approximated by the results of local optics for a one-step model. This amounts to ignoring the d-parameter corrections to the transmission amplitudes of transverse waves, which is typically an error of a few percent or less.[4,5] The resulting driving fields are sensitive to the (large) value of the speed of light in the sense that formally allowing c to increase decreases the size of

these fields but increases their spatial extent. Their integral over the normal coordinate is consequently insensitive to c, and to any screening imposed by Eq. (35) and to their truncation near the surface. Hence, for $|p_T|w, |p_T|/\kappa_0 \ll 1$, one can find a reasonable analytic approximation to the long-range contributions. To understand its form we write out the complex amplitude for the first-order, local optics, single-step, p-wave, electric field

$$\vec{E}_1 = \frac{cE_1}{\omega} e^{i(\mathbf{Q}\cdot\mathbf{X}-\omega t)} \times \begin{cases} (Q,-p_v,0)e^{ip_v x} + r(Q,p_v,0)e^{-ip_v x}, & x<0 \\ t(Q,-p_T,0)e^{ip_T x}, & 0<x. \end{cases} \quad (49)$$

Here p_T is the value of Eq. (46) in the bulk, $p_v = (\omega/c)\cos\theta$ is its value in vacuum, and $Q = (\omega/c)\sin\theta$. The triplet of numbers for each partial wave describes the field components along $\hat{x}$, $\hat{Q}$, and $\hat{t}$. By matching across $x=0$ with the standard boundary conditions of continuous $E_\parallel$ and $D_\perp$, one finds the Fresnel (local optics) results for the reflection and transmission amplitudes,

$$r = \frac{\epsilon_b p_v - p_T}{\epsilon_b p_v + p_T},$$

$$t = \frac{2p_v}{\epsilon_b p_v + p_T}. \quad (50)$$

From $\vec{E}_1$, one constructs $\vec{B}_1$ and $\vec{j}_1$, determines the long-range contributions to $\langle \hat{x}\cdot\vec{R}\rangle$, and integrates them (times $4\pi/\omega_b^2$) over $x>0$ to produce the long-range contribution to Γ_x for incident p waves,

$$\Gamma_x^{(p)} \sim (1+|r|^2)\cos^2\theta + \tfrac{1}{2}|t\,\sin\theta(\epsilon_b - 1)|^2. \quad (51)$$

Here $|r|^2$ is the reflection coefficient, and Eq. (51) looks like a (local-optics) momentum-balance result, plus a correction. But it is not the complete $\Gamma_x^{(p)}$, since we have so far ignored short-range contributions. These are by definition the terms remaining in Eq. (33) after the long-range contributions are removed.

This removal may be formally accomplished by letting $c\to\infty$; i.e., working in the nonretarded limit. In this limit the transverse wave vectors p_T and p_v vanish, while longitudinal wave vectors (for motion along $\hat{x}$)

$$p_L = \left(\frac{\tilde{\omega}^2 - \omega_0^2}{\beta_0^2} - Q^2 \right)^{1/2} \quad (52)$$

are scarcely modified by setting $Q\to 0$. This approximation is reasonable because the velocity parameter β_0 in metals is roughly two orders of magnitude smaller than c. It yields a short-range (one dimensional) form of Eq. (33),

$$\langle \hat{x}\cdot\vec{R}\rangle|_{c\to\infty} \to \langle R\rangle = -\left\langle j_1 \frac{\partial v_1}{\partial x}\right\rangle + \left\langle \frac{\rho_1}{\rho_0}\left(\frac{1}{\tau} j_1 + \frac{\beta_0^2}{3}\frac{\partial}{\partial x}\rho_1\right)\right\rangle. \quad (53)$$

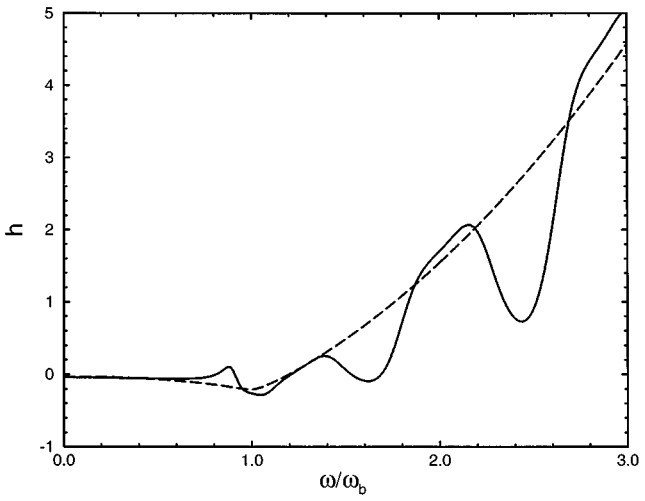

FIG. 7. Dimensionless h parameter vs frequency. The solid (dashed) curve is for a double- (single-) step model. These results, combined with Eq. (58), yield good agreement at any angle of incidence with the full calculations shown in Figs. 3 and 4.

Along with dropping the Lorentz force term here, all vectors have been replaced with their normal components. See the Appendix of Ref. 26 for a detailed rationale. The corresponding form of Eq. (32) is

$$0 = \frac{\omega_0^2}{4\pi}\langle E_2\rangle - \beta_0^2 \frac{\partial}{\partial x}\langle \rho_2\rangle + \langle R\rangle, \quad (54)$$

which is to be solved in a multistep model subject to the ABC's of continuity of $\langle E_2\rangle$ at each interface, and continuity of Eq. (28) at internal interfaces. Finally, we parametrize the integral over the second-order, short-range electric-field normal component by

$$-\int dx \langle E_2\rangle \equiv 4\pi|\sigma_1|^2 h/\rho_b, \quad (55)$$

where σ_1 is the first-order induced surface charge density, $\sigma_1 = \int dx\ \rho_1$. It is through σ_1 that one connects back to the full three-dimensional problem. Applying Gauss's law to Eq. (49) gives

$$4\pi\sigma_1 = \Delta(\hat{x}\cdot\vec{E}_1) = E_1 e^{i(\mathbf{Q}\cdot\mathbf{X}-\omega t)}\sin\theta[t-(1+r)], \quad (56)$$

which leads to

$$|4\pi\sigma_1|^2 = 8\pi\,\frac{\langle S\rangle}{c}\,|t\,\sin\theta(\epsilon_b - 1)|^2. \quad (57)$$

Substituting Eq. (57) into Eq. (55), and adding the result to Eq. (51) yields the approximate result

$$\Gamma_x^{(p)} = (1+|r|^2)\cos^2\theta + (\tfrac{1}{2}+2h)|t\,\sin\theta(\epsilon_b - 1)|^2. \quad (58)$$

Aside from the Fresnel amplitudes, one only needs the frequency-dependent parameter h to evaluate $\Gamma_x^{(p)}$.

We calculated the frequency dependence of h in our one- and two-step models. The results are shown in Fig. 7, and when combined with Eq. (58) provide a good approximation to the complete evaluations in Figs. 3 and 4. For the single-

step model h is a smooth function of frequency. Its limiting value as $\omega \to 0$ is $-\frac{1}{36}$, and its increase above ω_b is countered by the rapid decrease of $|\epsilon_b - 1|^2$ in Eq. (58). For the double-step model, h exhibits a multipole plasmon peak below ω_b and a sequence of scattering resonances above ω_b. These are responsible for most of the extra structure in Fig. 4 compared to Fig. 3. As for the accuracy of Eq. (58), note that only in the vicinity of the multipole peak does one see a slight discrepancy with the full calculation. Hence it appears that for $\Gamma_x^{(p)}$ one needs to focus just on the nonretarded, one-dimensional calculation of h, rather than to include the full set of Maxwell equations. This will greatly simplify quantum-mechanical treatments of the photon-drag emf along the surface normal, as it has for second-harmonic generation.[3]

We are setting up such calculations now, but will end our discussion by noting two cases where the quantum value of the h parameter is already known. To understand the connections note that, by Gauss's law, $\langle E_2 \rangle$ of the nonretarded problem obeys $(\partial/\partial x)\langle E_2 \rangle = 4\pi \langle \rho_2 \rangle$, so we may rewrite Eq. (55) as

$$h = \rho_b \int dx\; x \langle \rho_2 \rangle / |\sigma_1|^2. \tag{59}$$

There exists a special case where the required perturbed densities can be exactly calculated: a single, isolated surface of a parabolically confined electron gas.[27] For this special barrier the d parameters vanish at all frequencies, and the second-harmonic a parameter is exactly -2. From Eq. (59) we obtain the additional exact result $h(\omega) = -\frac{1}{4}$. This implies, via Eq. (58), that $\Gamma_x^{(p)}$ for this system is given by the momentum-balance result, $\Gamma_x^{(p)} = (1 + R^{(p)})\cos^2\theta$, with no surface-sensitive corrections.

The other case where we can relate h to known results is in the low-frequency limit. As $\omega \to 0$, it does not matter whether one is calculating ρ_2 at 2ω or static. We can hence relate h to the a parameter of second-harmonic generation [noting Ref. 16 and Eq. (CS-15)]:

$$h(\omega = 0) = \tfrac{1}{8} a(\omega = 0). \tag{60}$$

From Table I in Ref. 3, which lists $a(\omega = 0)$ for various models, we see that our hydrodynamic results are too small in magnitude by about a factor of 100. Using better (more negative) values of h from the quantum evaluations of density response will make $\Gamma_x^{(p)} < 0$, at least over a range of low frequencies and at larger angles of incidence. This sign change arises from short-range forces near the surface. At $\omega = 0$, j_1 vanishes so the only driving term in Eq. (53) is $+(\beta_0^2/6\rho_0)(\partial/\partial x)\langle \rho_1^2 \rangle$, which is strictly positive in a one-step hydrodynamic model. This leads in turn to a negative $\langle E_2 \rangle$, which means that, in second-order, electrons have been pulled toward the surface by the light; i.e., in the opposite direction from what one expects due to radiation pressure. The hydrodynamic model obtains the right sign of this effect, but badly underestimates its magnitude.[3,28]

D. Conclusions

Our various model calculations have shown that simple estimates from momentum balance arguments can give exact results in special cases. However, there are also situations where their predictions are qualitatively wrong. For instance, a suitable variation of the electron relaxation rate as a function of depth into the metal can lead to a reversed direction for the surface-parallel current. With the emf induced along the surface normal, the sign and magnitude of the effect is a sensitive function of the equilibrium electron-density profile and microscopic quantum-mechanical calculations will be needed to give reliable predictions. These should be tractable with the h-parameter approach we have outlined.

[1] M. Corvi and W. L. Schaich, Phys. Rev. B **33**, 3688 (1986).
[2] A. V. Petukhov, Phys. Rev. B **52**, 16 901 (1995).
[3] A. Liebsch and W. L. Schaich, Phys. Rev. B **40**, 5401 (1989).
[4] A. Liebsch, *Electromagnetic Waves: Recent Developments in Research, Vol. 2: Photonic Probes of Surfaces* (Elsevier, New York, 1995).
[5] A. Liebsch, *Electronic Excitations of Metal Surfaces: Applications of Local Density Theory* (Plenum, New York, 1997).
[6] A. Grinberg, *The Discovery of the Photon-Drag Effect* (Delphic Associates, Falls Church, VA, 1986).
[7] V. M. Shalaev, C. Douketis, J. T. Stuckless, and M. Moskovits, Phys. Rev. B **53**, 11 388 (1996).
[8] V. L. Gurevich, R. Laiho, and A. V. Lashkul, Phys. Rev. Lett. **69**, 180 (1992).
[9] V. L. Gurevich and R. Laiho, Phys. Rev. B **48**, 8307 (1993).
[10] V. L. Gurevich and A. Thellung, Physica A **188**, 654 (1992).
[11] A. Thellung, *Proceedings of the XXIX Winter School of Theoretical Physics*, edited by T. Paszkiewicz and K. Rapcewicz (Plenum, New York, 1993).
[12] R. K. Wangsness, *Electromagnetic Fields* (Wiley, New York, 1986), p. 425.
[13] R. Laiho, Phys. Rev. B **52**, 15 054 (1995).
[14] J. D. Jackson, *Classical Electrodynamics* (Wiley, New York, 1975), p. 236.
[15] Equation (n) in Ref. 1 will be referred to as (CS-n).
[16] F. Forstmann and R. R. Gerhardts, *Metal Optics Near the Plasma Frequency*, Springer Tracts of Modern Physics Vol. 109 (Springer, New York, 1986).
[17] A. J. Bennett, Phys. Rev. B **1**, 203 (1970).
[18] J. A. Maytorena, W. L. Mochan, and B. S. Mendoza, Phys. Rev. B **51**, 2556 (1995).
[19] This distinction was missed in W. Schaich, Solid State Commun. **88**, 5 (1993). The numerical results there for optical rectification are hence quantitatively, but not qualitatively, in error.
[20] P. Halevi, Phys. Rev. B **51**, 7497 (1995).
[21] For constant τ but arbitrary n_0, Eq. (3) is exact.
[22] F. Forstmann and H. Stenschke, Phys. Rev. B **17**, 1489 (1978).
[23] A. D. Boardman, in *Electromagnetic Surface Modes*, edited by A. D. Boardman (Wiley, New York, 1982), p. 1.
[24] This agreement is in contrast to the behavior of maxima in second-harmonic generation—see Fig. 4 in Ref. 1.
[25] There are also singular (δ-function) contributions, specifically from $\langle (\vec{j}_1 \cdot \vec{\nabla})(\hat{Q} \cdot \vec{v}_1) \rangle$ at internal points where τ is discontinuous.
[26] W. L. Schaich and A. Liebsch, Phys. Rev. B **37**, 6187 (1988).
[27] W. L. Schaich, Surf. Sci. **318**, 6187 (1988).
[28] M. Weber and A. Liebsch, Phys. Rev. B **35**, 7411 (1987).